Scaling of single-bubble growth in a porous medium

C. Satik,* X. Li, and Y. C. Yortsos†
Petroleum Engineering Program, Department of Chemical Engineering, University of Southern California, Los Angeles, California 90089-1211
(Received 7 November 1994)

Mass-transfer driven growth of a single gas cluster in a porous medium under the application of a supersaturation in the far field is examined. We discuss the growth pattern and its growth rate. Contrary to compact (spherical) growth in the bulk, growth patterns in porous media are disordered and vary from percolation to diffusion-limited aggregation (DLA) as the cluster size increases. At conditions of low supersaturation, scaling laws for the boundaries that delineate these patterns and of the corresponding growth rates are derived. In three dimensions (3D), it is found that the cluster grows as $R_g \sim t^{1/(D_f-1)}$, where D_f is the pattern fractal dimension (≈ 2.50 for percolation or DLA). A similar result involving logarithmic corrections is found for 2D. These results generalize the classical scaling $R_g \sim t^{1/2}$ to fractal clusters.

PACS number(s): 47.55.Mh, 05.40.+j, 68.35.Fx, 44.30.+v

I. INTRODUCTION

Many processes in porous media involve a liquid-to-gas phase change. Examples include the recovery of oil from underground reservoirs by the process of "solution gas-drive" and geothermal and enhanced heat transfer processes [1]. The first involves the release of a volatile component ("solution gas") from the oleic phase, upon the sudden or gradual reduction of pressure, to form a gas phase that displaces the liquid. The latter typically involve the boiling of a single-component liquid. Invariably, a number of nucleation centers exist on the pore surface [2]; thus the growth of the gas phase takes place from a multitude of clusters. Contrary to the compact patterns in gas phase growth in the bulk or in a Hele-Shaw cell [3], however, bubble growth patterns in porous media are disordered. As in the related problem of external immiscible displacement in porous media [4], they reflect the underlying pore microstructure. The competition between multiple clusters is also different than it is in the bulk. At least under conditions where capillary forces dominate, gas-liquid interfaces in porous media assume the curvature of the pore throats that they occupy; thus capillary effects in a gas cluster are not directly related to an equivalent effective radius of curvature, as is the case for spherical bubbles in the bulk. The emerging cluster patterns, for example, of the percolation type [5], affect significantly the rates of mass transfer and the growth of individual clusters. Furthermore, processes such as Ostwald ripening, which depend strongly on the local interface curvature, are also expected to play a role different than they do in the bulk.

To characterize bubble growth in porous media, two aspects must be determined: the growth patterns and the rates of growth. In the bulk or in an effective medium (such as a Hele-Shaw cell) these patterns are compact (for instance, radial or spherical, in the absence of gravity and under symmetry conditions) and growth of an isolated single bubble obeys the similarity scaling [3] $R \sim t^{1/2}$. In a random porous medium, however, we expect a percolation pattern at small cluster sizes and a viscous fingering pattern at larger sizes, both of which would have a significant effect on the scaling of single and multiple clusters. The delineation and growth of these regimes for an isolated bubble (cluster) form the main objective of this paper. As in other displacement processes in porous media, useful information can be obtained by visualization experiments in model porous media.

In a recent study [5] we reported on the visualization of bubble growth in two-dimensional (2D) etched glass micromodels, where the evolution of CO_2 gas from a supersaturated carbonated water was studied. Figure 1(a) shows a typical snapshot of this process for an experiment in which the liquid pressure was suddenly reduced from its saturated value of 50 to 14.7 psi. The displaced liquid flows out of the micromodel through two outlet ports, situated in the middle of the two lateral sides. The snapshot in Fig. 1(a) corresponds to the time when a "sample-spanning cluster" is about to form. The pattern is clearly disordered and nonsymmetric. Of significant interest is the mechanism of growth of the individual clusters. At least during the early stages of the experiments, isolated clusters were found to grow in a manner similar to external drainage: the locally spherical gas-liquid interfaces [Fig. 1(b)] advanced slowly (or not at all) in the converging portion of a pore throat, and then rapidly moved to occupy an adjacent pore (in an event know as a "rheon" [4]) once they reached the smallest constriction of the throat, at which time the capillary pressure barrier of that throat was exceeded [second snapshot of Fig. 1(b)]. This "one-pore-at-a-time" mechanism of growth is typical of invasion percolation [4] (although in

*Present address: Department of Petroleum Engineering, Stanford University, Stanford, CA 94305-2220.
†Author to whom correspondence should be addressed.

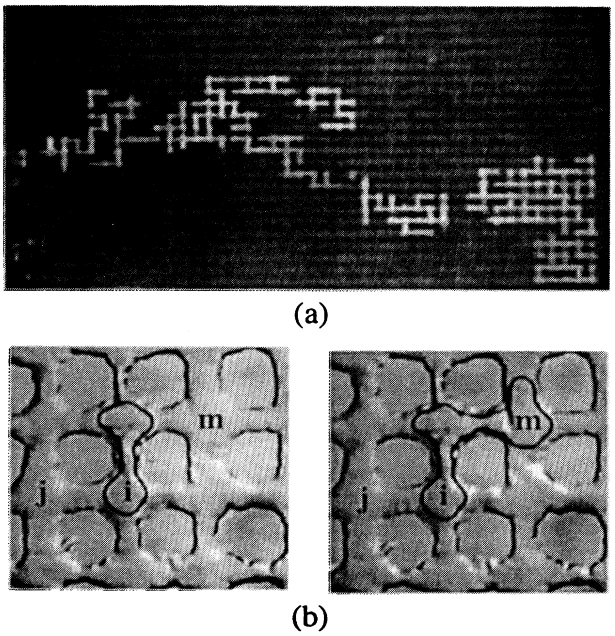

FIG. 1. Experimental snapshots of gas cluster growth from carbonated water in a glass micromodel: (a) large scale; (b) pore scale sequence.

the present case of solute diffusion, the interface movement is much slower than in typical external displacements). At later stages, more than one pore of a single cluster was simultaneously filled, indicating that capillary forces became less controlling, while snap-off of gas bubbles accompanied the breakthrough of gas at the outlet ports.

While multiple cluster growth is very important, as discussed elsewhere [5], the simpler problem of single-bubble growth is still not well understood and must be investigated. This forms the subject of this paper. We consider single-bubble (cluster) growth in a porous medium, schematically shown in Fig. 2, driven by a far-field supersaturation. The analysis will focus first on the case of a fixed supersaturation. Subsequently, it will be generalized to the more usual case of a gradual increase in the supersaturation. The two related applications, namely growth by diffusion of a volatile component in a binary liquid, driven by pressure lowering, or by heat conduction in a single-component liquid, driven by a temperature increase, will be uniformly treated. However, in the remainder of this paper use will be made of the terminology of the first problem. Our emphasis is on the development of a theory of growth at low supersaturations, where diffusion dominates the growth and convection effects are secondary. Furthermore, and for simplicity, we assume that effects of gravity are negligible and that the kinetics at the gas-liquid interface are sufficiently fast for thermodynamic equilibrium to prevail [6]. As is conventional, we take the porous medium to consist of a network of distributed-size bonds (throats) and sites (pores), where we associate transport and capillary resistance with bonds and volumetric storage with sites.

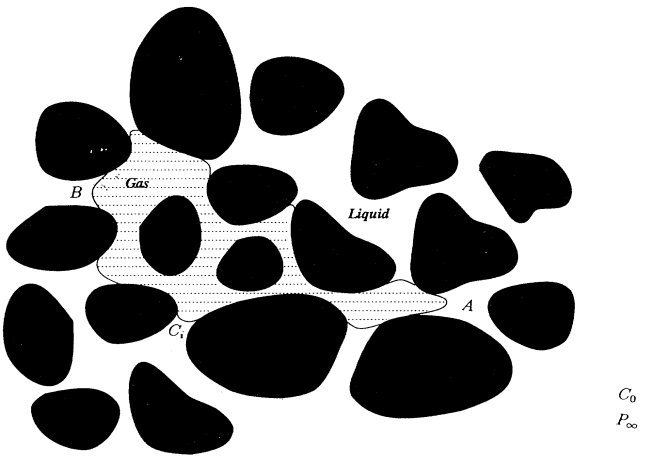

FIG. 2. Schematic of gas bubble growth in a porous medium. C_0, P_∞ are far-field concentration and pressure, C_i is equilibrium concentration corresponding to P_∞.

The paper is organized as follows: First, a theory is developed that delineates the region of applicability of the two limiting growth patterns, namely percolation and diffusion-limited aggregation (DLA), under conditions of low supersaturation. The theory uses scaling arguments. Subsequently, the rates of growth corresponding to the two regimes are derived. Then, a pore network numerical model that simulates multiple cluster growth, the details of which are given elsewhere [5], is used to test the theoretical predictions. We also comment on the applicability of the theory and its extension to the case of a variable far-field supersaturation.

II. THEORY

Consider the growth of a single gas cluster from a binary liquid in a porous medium (Fig. 2). The liquid is initially at saturated conditions, such that before the formation of the gas cluster we have uniform concentration and pressure, $C = C_0$ and $P_l = P_0 \equiv KC_0$, where C denotes the volatile solute concentration, P_l is the liquid pressure, and K is the solubility constant. At time $t = 0$, the far-field pressure P_∞ is suddenly reduced, $P_\infty < P_0$, to create a far-field supersaturation, $(P_0 - P_\infty)/P_0$, which remains constant thereafter. A generalization to the case of an increasing supersaturation is also discussed later. As a result of the imposed supersaturation, nucleation of a single gas cluster is assumed. Issues of nucleation in porous media were discussed in Refs. [2], [5], and [7], where it was pointed out that nucleation is likely to be of a heterogeneous nature and to be controlled by pore surface nonuniformities . In the present context, we will proceed by assuming the formation of only one cluster, which, without loss in generality, we take to occur at the onset of pressure decline, $t = 0$. Because we are considering a single cluster at a fixed supersaturation, this cluster would grow continuously. This is in contrast to the multiple cluster problem, where the competition between various clusters determines which cluster and at what rate it grows [5].

Isothermal conditions are assumed throughout the pro-

cess. In a separate study [8] we have also considered the related problem of the growth of a vapor bubble in a single-component liquid, with the application of a constant heat flux, where heat transfer (also involving solid heat conduction) controls the process. Because the far-field pressure is assumed to be uniform, no external velocity field is applied. It should be noted, however, that in some practical applications bubble growth may take place under conditions of an externally applied velocity field, which is induced by the production of the liquid phase considered as slightly compressible. This interesting case will not be considered here. In our context, liquid is produced only as a result of its immiscible displacement by gas. Under typical conditions, gas can be considered as the nonwetting phase; hence the process should share many of the characteristics of drainage. Before we proceed with the scaling theory, we first describe some general features of the problem.

Without loss in generality, we take the gas to be inviscid and ideal, so that the gas pressure P_g is spatially uniform and the ideal gas law applies,

$$P_g V_g = n\mathcal{R}T \ , \tag{1}$$

where V_g denotes the volume of the gas cluster, n is the number of moles of solute in the gas phase, $\mathcal{R}$ is the ideal gas constant, and T is the temperature (also assumed constant). For simplicity we assume that only one component vaporizes and that thermodynamic equilibrium at the gas-liquid interface at any perimeter site i follows a linear law

$$P_g = KC_i \ . \tag{2}$$

Here, the subscripts g and i refer to gas phase and perimeter site, respectively. Thus, in the absence of liquid flow, the equilibrium concentration at the cluster interface is proportional to the far-field pressure $C_i = P_\infty / K$. All these assumptions are for the sake of convenience and do not detract from generality.

The gas cluster is delineated by the gas-liquid interface (menisci) at the cluster perimeter, the curvature of each of which is dictated by the local pore geometry [see, for example, Fig. 1(b)]. Under the assumption of thermodynamic equilibrium at the interface, bubble growth is controlled by the net mass transfer rate to the cluster

$$\frac{dn}{dt} = \sum_{i,j} J_{ij} \ , \tag{3}$$

which occurs to all perimeter menisci, whether moving or stationary. In the above, we have used the subscript j to denote all liquid-occupied sites adjacent to a perimeter site i, and the sum is over all such i and j. The net molar flow rate J_{ij} can be approximated by

$$J_{ij} \approx D A_{ij} \frac{(C_i - C_j)}{l} \ , \tag{4}$$

where D is solute diffusivity, l is the network spacing (bond length) assumed constant, and the area A_{ij} pertains to bond ij connecting the adjacent sites i and j. The concentration field can be found by considering mass transfer in the liquid, which at conditions of small supersaturation is diffusion limited. This regime is known as the *quasi-static* limit [5,9]. Convective effects are important in the boiling application [8] and at higher supersaturations, and their scaling is discussed in [8].

It follows from (1) that a positive mass influx ($dn/dt > 0$) results in either pressurization ($dP_g > 0$) or bubble growth ($dV_g > 0$). Pressurization is necessary to overcome the capillary pressure barrier of a perimeter bond before the cluster can grow. For an arbitrary bond ij [Fig. 1(b)], this occurs when the capillary pressure P_c first reaches the capillary pressure barrier

$$P_{c,ij} \equiv P_g - P_{l,j} = \frac{2\gamma}{r_{p,ij}} \ , \tag{5}$$

where $r_{p,ij}$ is the bond radius and γ denotes interfacial tension. Upon penetration, the interface advances and occupies site j, during which time capillary effects are negligible. Before this event, the meniscus advances slowly (if at all) in the converging geometry portion of the pore throat. A dimensional analysis of the above equations shows that dimensionless groups of relevance [5] are the *Jakob* number

$$\mathrm{Ja} = \frac{P_0 - P_\infty}{P_0} \ , \tag{6}$$

which conventionally expresses supersaturation, the capillary number

$$\mathrm{Ca} = \frac{\mathrm{Ja} D l \mu}{\gamma k} \ , \tag{7}$$

where μ is liquid viscosity and k is permeability. Expression (7) for Ca differs from the conventional one for external displacements [4], $\mathrm{Ca} = u\mu/\gamma$, in that the characteristic velocity here is based on diffusion, $u = \mathrm{Ja} D l / k$. We also note that as the permeability is another measure of an average pore size (recall the scaling [10] $k \sim r_p^{*2}$, where r_p^* is a characteristic size) the above velocity expresses diffusion-induced flow across a typical pore. Next, we proceed with the description of patterns and rates of growth and their scaling.

A. Growth patterns

1. Percolation

At small sizes, we expect the cluster to grow following a percolation pattern, where perimeter bonds are invaded "one at a time," such that the largest perimeter bond is always invaded first. This mode of interface advance is similar to *invasion percolation* in external displacements, except that here accessibility to an internal (nucleation) site, rather than an external site, is required. For percolation patterns to be applicable, the following must hold: (i) During pressurization (where only P_g increases), all interfaces are stationary (or slowly advancing) and stable. (ii) During growth (filling step), only one pore throat is invaded to fill the adjoining site. Both these

conditions were observed in our visualization experiments and are expected to apply for sufficiently small sizes, as discussed below. It should be pointed out that percolation rules can also be applicable in the multiple cluster growth problem, where growth in each cluster may also follow the "one-site-at-a-time" rule. The exception is that in that problem, although the bond to be penetrated next in any given cluster is the one with the smallest capillary barrier among all other perimeter bonds of this cluster, it is not necessarily the one with the smallest barrier *over all* clusters. This is a consequence of the competition among clusters and the mass transfer, as discussed in more detail in Ref. [5].

In deriving the limits of the percolation pattern, we first note that condition (i) is always satisfied, since during the pressurization step all interfaces reside in converging pore geometries [Fig. 1(b)] and fluid flow is negligible. On the other hand, the validity of (ii) depends on the relative magnitude of viscous and capillary forces. For example, consider the filling of a site [(e.g., site m in Fig. 1(b)]. For the pattern to follow invasion percolation rules, the simultaneous penetration of another site j should not be possible during this invasion step; namely, the condition $P_{c,ij} < 2\gamma / r_{p,ij}$ must apply for all other perimeter bonds and adjacent sites. Now, due to liquid displacement from site m, a viscous pressure drop develops in the liquid. Assuming that during the filling step capillary effects are insignificant, or that $P_g \approx P_m$, enforcement of the above condition requires that the viscous pressure drop between site m and any other site j adjacent to the perimeter be small:

$$\Delta P_v = P_m - P_{l,j} < \frac{2\gamma}{r_{p,ij}} . \tag{8}$$

This condition is likely to be violated at sufficiently large cluster sizes, in which case two sites of the same cluster would be simultaneously penetrated. Then, the occupancy sequence would also be dictated by the magnitude of the vicous forces, and the problem is not strictly invasion percolation. It can be noted here that at modified form of the latter in terms of gradient percolation [11] or a variation could be used to describe this problem, but this possibility will not be explored here. In the following, we shall denote by R^p (percolation boundary) the size of the cluster when deviation from a strictly percolation pattern first occurs and proceed with its delineation in terms of the capillary number.

To estimate viscous effects, the pressure field must be related to the mass transfer. Because in the percolation regime growth occurs from one site only (denoted above by m), although mass transfer continues to all perimeter sites, all pressures in the liquid are set by the displacement velocity in the growth site v_m. To obtain an expression for the latter, first we take the derivative of (1) at constant pressure and combine it with (2) to get

$$v_m \approx \frac{RT}{bP_\infty} \sum_{i,j} J_{ij} . \tag{9}$$

Here, b is a geometrical factor that accounts for the different geometries in two and three dimensions, $b = 2\pi h r_s^*$ in 2D and $b = 4\pi r_s^{*2}$ in 3D, respectively, where h denotes thickness in 2D (e.g., the micromodel thickness) and r_s^* is a typical site radius. Within some constants of proportionality, b is of the same order of magnitude in both geometries. The subscript s refers to sites. The next step involves expressing J_{ij} in terms of the mass transfer in the liquid. In general, mass transfer occurs by convection and diffusion. As noted above, however, here we consider the limit of *low supersaturation* (Ja $\ll 1$), where convection is negligible and the concentration field is quasistatic [5,9]. Therefore, the problem reduces to solving the Laplace equation

$$\nabla^2 C = 0 \tag{10}$$

in the liquid-occupied Euclidean space, which is bounded on one side by the self-similar fractal interface of the growing cluster. The appropriate boundary conditions are constant concentration $C = C_i$ at the fractal interface and $C = C_0$ in the far field. The solution of this problem is greatly aided by an analogous problem considered in Ref. [12]. There, it was shown that the total flux to the fractal interface is identical to that obtained from the solution of the corresponding mean-field problem, where a compact circle (or sphere) of an equivalent radius R_g replaces the fractal interface. We follow the same approach to find, after some calculations, the result

$$\sum_{i,j} J_{ij} \approx 2\pi h D R_g \left. \frac{\partial C}{\partial r} \right|_{r=R_g} = \frac{2\pi h D (C_0 - C_i)}{\ln(R_e / R_g)} \tag{11}$$

in 2D geometries, where R_e is the outer boundary, assumed finite, and

$$\sum_{i,j} J_{ij} \approx 4\pi D (C_0 - C_i) R_g \tag{12}$$

in 3D geometries, respectively. Because our interest is in the determination of the percolation boundary R^p, we consider in particular the application of (11) and (12) in the limit $R_g = R^p$. Use in (9) then gives

$$v_m \approx \left[\frac{\alpha \mathrm{Ja} D}{r_s^*} \right] \frac{1}{\ln(R_e / R^p)} \tag{13}$$

in 2D and

$$v_m \approx \left[\frac{\alpha \mathrm{Ja} D}{r_s^*} \right] \left[\frac{R^p}{r_s^*} \right] \tag{14}$$

in 3D, respectively, and we have defined the solubility parameter $\alpha = \mathcal{R}T / M_w K$, where M_w is the solute molecular weight. The diffusive scaling of the growth velocity should be noted.

The final step is to determine the viscous pressure drop from a knowledge of the velocity at the growing site. For a conservative estimate, we evaluate ΔP_v across a distance of the same order as R^p. Since the flow resistance across each pore can be approximated by Poiseuille's law, the pressure field also satisfies a Laplace equation, provided that the distribution of pore sizes is not too wide to introduce critical paths of the type discussed in Ref. [10]. This problem is also analogous to the previous one, except that now the internal boundary condition is one of a specified flow (velocity) at a point (the growth site) in-

stead of a constant pressure. We use a mean-field approach (which, incidentally, was also taken in the related study [13] of external displacement) and consider radial flow from a point source. After some calculation (see Appendix) we obtain

$$\Delta P_v \approx \frac{2v_m \mu r_s^*}{k} \ln \frac{2R^p}{r_s^*} \tag{15}$$

in 2D and

$$\Delta P_v \approx \frac{v_m \mu r_s^*}{k} \tag{16}$$

in 3D geometries, respectively. Note that in (15) and (16) we used the permeability as an approximation of the effective flow conductivity. Finally, substitution of the velocity from (13) and (14) leads to

$$\Delta P_v \approx \frac{2\alpha\mu \mathrm{Ja} D}{k} \frac{\ln \frac{2R^p}{r_s^*}}{\ln \frac{R_e}{R^p}} \tag{17}$$

and

$$\Delta P_v \approx \frac{\alpha\mu \mathrm{Ja} D}{k} \frac{R^p}{r_s^*} , \tag{18}$$

which clearly show the mass-transfer origin of the viscous pressure drop in this problem.

We are now in a position to estimate R^p. To proceed we follow Ref. [13] and request that variations in the number of the gas cluster sites N_g due to the possible penetration of more than one site at a time, are small

$$\frac{\Delta N_g}{N_g} = \epsilon \ll 1 , \tag{19}$$

where ϵ is a small positive number. Because the cluster is of the percolation type, this is equivalently expressed [13] as

$$\frac{\Delta N_g}{N_g} = \beta (p - p_c)^{-1} \Delta p , \tag{20}$$

where β is the percolation probability exponent, p is the percolation probability corresponding to the particular capillary pressure level at this stage, and p_c is the percolation threshold of the lattice. We recall that in external drainage, p is related to the throat size distribution $\alpha_p(r_p)$ via

$$p = \int_{r_p}^{\infty} \alpha_p(r) dr , \tag{21}$$

thus

$$\Delta p \approx \alpha_p(r_p) \Delta r_p \approx \frac{\Delta r_p}{\sigma r_p} , \tag{22}$$

where σ is a dimensionless measure of the standard deviation of α_p. Furthermore, because of (5), variations in the size of penetrated pores are related to those in capillary pressure,

$$\Delta P_c \sim \frac{2\gamma \Delta r_p}{r_p^2} , \tag{23}$$

and because the gas pressure is uniform, to the viscous pressure drop

$$\Delta P_c \approx \Delta P_v . \tag{24}$$

Using (20)–(24) we can relate ΔP_v to ΔN_g as follows:

$$\frac{\Delta N_g}{N_g} = \frac{\beta r_p}{2\gamma\sigma(p - p_c)} \Delta P_v . \tag{25}$$

Equivalently, we may substitute $(p - p_c)$ by approximating the size of the cluster R^p with the percolation correlation length

$$\frac{R^p}{l} \approx \xi \sim (p - p_c)^{-\nu} , \tag{26}$$

where the correlation length exponent ν equals $\frac{4}{3}$ in 2D and 0.88 in 3D. Then, a final substitution in (19) gives the results

$$\left(\frac{R^p}{l} \right)^{1/\nu} \left(\frac{\ln \frac{2R^p}{r_s^*}}{\ln \frac{R_e}{R^p}} \right) \frac{\alpha\beta \mathrm{Ca}}{\sigma} \sim \epsilon \frac{l^*}{r_p^*} \sim \epsilon \tag{27}$$

in 2D and

$$\left(\frac{R^p}{l} \right)^{1/\nu+1} \frac{\alpha\beta \mathrm{Ca}}{2\sigma} \sim \epsilon \frac{r_s^*}{r_p^*} \sim \epsilon \tag{28}$$

in 3D geometries, respectively. In the above equations the right-hand side was simplified by using the fact that the various pore length scales involved are of the same order of magnitude. Equations (27) and (28) delineate the boundaries of percolation growth patterns in the respective dimensions. These equations are analogous, although not the same, to the expression that delineates percolation boundaries in external drainage developed for 2D geometries [13]. It is clear from the two equations that the cluster size at the percolation limit decreases as Ca increases, namely as Ja or D increase. Accordingly, and under the assumption of diffusion control, strictly percolation patterns set in at smaller cluster sizes as the supersaturation becomes larger.

2. *Viscous fingering*

When the cluster size increases beyond R^p, the pattern departs from percolation. From a linear stability analysis of the equivalent problem in an effective porous medium (or a Hele-Shaw cell) Li and Yortsos [3] found that in the limit of negligible capillarity, the problem possesses the Mullins-Sekerka instability of solidification [14], which in a porous medium also happens to coincide exactly with the viscous fingering instability. Therefore, we expect that a DLA pattern would emerge at sufficiently large sizes. This was indeed confirmed by numerical simulations, as shown below. To delineate the boundary of this pattern, R^{vf}, we proceed as before, except that now we

must request that variations in the capillary pressure be *small* compared to viscous pressure drop

$$\Delta P_c = \epsilon \Delta P_v \ . \tag{29}$$

For a conservative estimate we take the pressure drop between *adjacent* sites, which using the previous approach is given by

$$\Delta P_v \approx \frac{v_m \mu r_s^*}{k} \ln 2 \tag{30}$$

in 2D and

$$\Delta P_v \approx \frac{v_m \mu r_s^*}{2k} \tag{31}$$

in 3D, respectively. Substitution of v_m from (13) and (14) leads to the final results

$$\left[\frac{1}{\ln \frac{R_e}{R^{vf}}} \right] \left[\frac{\alpha \mathrm{Ca}}{\sigma} \right] \sim \epsilon^{-1} \tag{32}$$

in 2D and

$$\left[\frac{R^{vf}}{l} \right] \left[\frac{\alpha \mathrm{Ca}}{\sigma} \right] \sim \epsilon^{-1} \frac{r_s^*}{l} \sim \epsilon^{-1} \tag{33}$$

in 3D geometries, respectively. These equations define the boundaries of the viscous fingering growth pattern in the respective geometries. Clearly, larger values of Ca promote a pure DLA growth pattern at smaller cluster sizes.

In summary, Eqs. (27) and (28), and (32) and (33), delineate the boundaries of the two limiting growth patterns in the absence of effects, such as snap-off, gravity, etc. Implicit in their derivation is the assumption that the cluster size is sufficiently large (compared to the lattice spacing) for statistical theories, such as percolation, to be meaningful, yet sufficiently small (compared to the outer boundary) for the radially symmetric mean-field results to apply. These restrictions are important in the numerical simulations, as discussed below.

B. Rates of growth

The other important aspect in single-bubble growth involves rates of growth. For their determination we shall make use of the previous theory. Let V_s denote the average volume of a site, which we will take as a constant for the sake of simplicity. Then, a direct mass balance on the displaced liquid gives the result

$$V_s \frac{dN_g}{dt} = v_m b \ , \tag{34}$$

which can be rewritten in terms of the cluster radius R_g, with the use of

$$N_g \sim \left[\frac{R_g}{l} \right]^{D_f} \ , \tag{35}$$

where D_f is the mass fractal dimension. Substitution of v_m from (13) and (14) gives a differential equation, the integral of which reads

$$\left[\frac{R_g}{l} \right]^{D_f} \left[1 + D_f \ln \frac{R_e}{R_g} \right] \approx \frac{D_f \alpha b \mathrm{JaD}}{V_s r_s^*} t \sim \frac{\alpha \mathrm{JaD}}{k} t \tag{36}$$

in 2D and

$$\left[\frac{R_g}{l} \right]^{D_f - 1} \approx \frac{(D_f - 1)}{D_f} \frac{\alpha b l \mathrm{JaD}}{V_s r_s^{*2}} t \sim \frac{\alpha \mathrm{JaD}}{k} t \tag{37}$$

in 3D geometries, respectively. In the right-hand side of the above we have used $\sqrt{k}$ as the common characteristic length in order to obtain an order-of-magnitude estimate. Equations (36) and (37) express the rate of growth of the mean cluster size as a function of time and the applied supersaturation. The two scalings should be contrasted with the classical one for growth in the bulk [3], $R_g^2 \sim t$. It is clear that as a result of its ramified structure in the porous medium ($D_f < 3$), the cluster grows faster than its effective medium analog. For example, we have $R_g \sim t^{2/3}$ for the 3D case in either the percolation or the viscous fingering limits (where $D_f \approx 2.50$). In either geometry, the growth is accelerated at higher values of the supersaturation Ja, the diffusion coefficient D, and the solubility parameter α.

III. SIMULATIONS

To test the above theory we use the numerical simulator developed for 2D geometries as described in Ref. [5]. This simulator solves for the viscous pressure field in the liquid during displacement and for mass transfer (including convection) during both pressurization and pore-filling steps. Menisci are allowed to penetrate a bond, if their capillary barrier is exceeded. Because of the complexity of the simulations, however, the computational requirements are large. As a result, bubble growth simulations were performed in 2D square lattices of small sizes. First, the mean-field result for the flux to a percolation cluster [Eq. (11)] was tested (Fig. 3). Here, we used a successive overrelaxation technique (SOR) to solve the

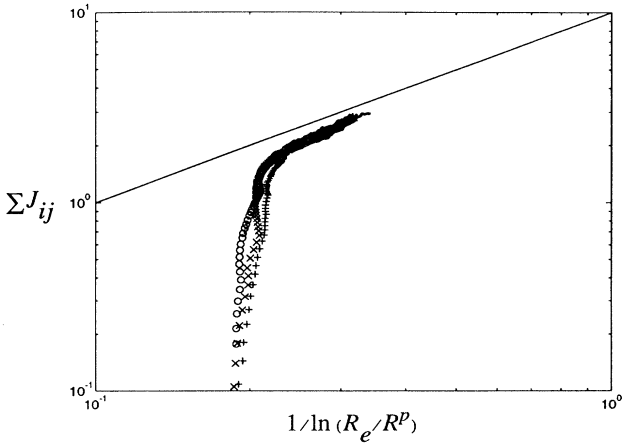

FIG. 3. Total net flux to a percolation cluster under quasi-static diffusion. The solid line is the theoretical slope [Eq. (1)].

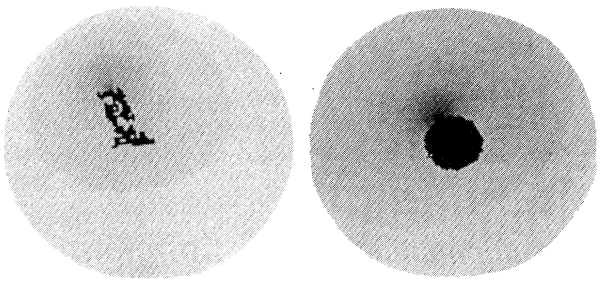

FIG. 4. Pressure fields corresponding to bubble growth: (a) full numerical simulation; (b) mean-field result.

Laplace equation outside a percolation cluster of variable size, which was grown following percolation rules. Good agreement with the mean-field theory was found (Fig. 3), provided that the computational size was sufficiently large (200×200 in Fig. 3) and the cluster size was also sufficiently large, but not too large for the boundary to affect the radial symmetry. Indeed, the segment of the curve that agrees with the theoretical scaling is shown to lie in the intermediate interval $l \ll R \ll R_e$. We expect that the window of applicability of the mean-field results would increase as the lattice size increases and as we use 3D lattices. To test the other mean-field results on the fluid flow, we compared constant pressure curves obtained at a stage of the full simulation of bubble growth [Fig. 4(a)] to those obtained by the mean-field theory (Appendix) for a comparable mean size [Fig. 4(b)]. The two fields are qualitatively similar, although quantitative differences do exist due to the finite size of the computational domain.

Next, simulations of the two pattern boundaries R^p and R^{vf} were conducted in smaller size lattices. Results for a 50×50 lattice are shown in Fig. 5, where only quasistatic diffusion was considered. It was pointed out above that the simulator also accounts for convection and transients [5]. However, various simulations at low Ja did not produce results appreciably different from those of quasistatic diffusion, the solution of which is computationally much faster. As shown in Fig. 5, the qualitative trend of the numerical results is consistent with the theory. However, due to the small lattice size and the associated finite-size effects (which are already present in the less demanding problems of Figs. 3 and 4), a quantitative agreement is difficult to ascertain. Certainly, a better agreement would be expected as the size increases to at least 200×200 (compare with Fig. 3). Figure 6 shows a log-log plot of quantity A [related to the percolation boundary as shown in (38)] vs Ca from a simulation in a 200×200 lattice, where

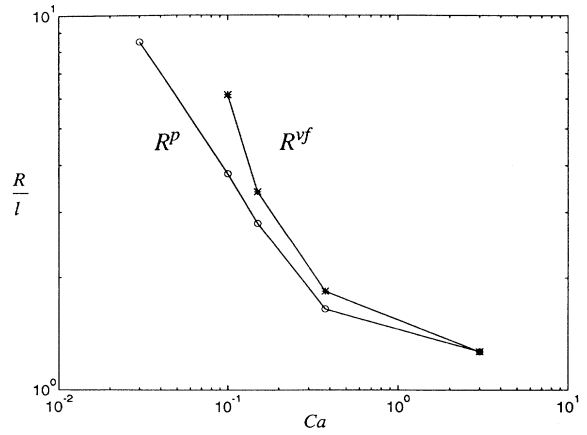

FIG. 5. Percolation and viscous fingering boundaries from pore network simulations in a 50×50 square lattice. The solid line is a guide to the eye.

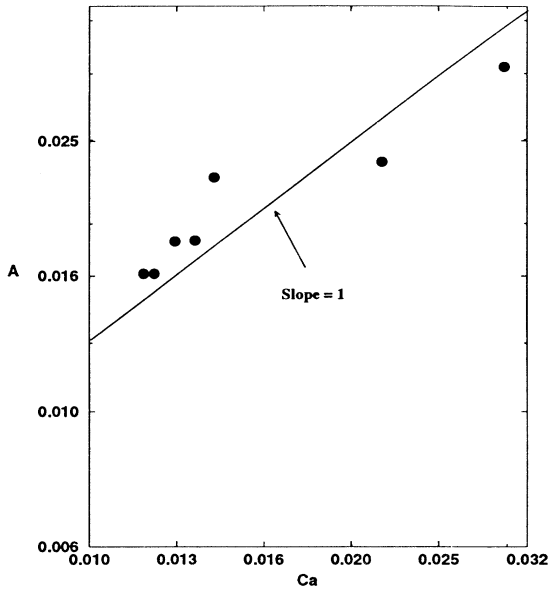

FIG. 6. Plot of the percolation boundary parameter A defined in Eq. (38) vs Ca.

$$A = \left[\frac{l}{R^p}\right]^{1/\nu} \left[\frac{\ln\frac{R_e}{R^p}}{\ln\frac{2R^p}{r_s^*}}\right] . \tag{38}$$

From (27) we expect the log-log plot to be a straight line of slope 1. Because of strong finite-size effects at the two limits of large Ca, where the cluster is too small for percolation theory results to be significant, and of small Ca, where the cluster/domain size ratio is sufficiently large for strong interference from the boundary, the plot covers only a small interval in Ca. The data fall reasonably close to a straight line, as expected. In all cases tested, fully consistent with the theory was the fact that different data for various combinations of viscosity, interfacial tension, diffusivity, and supersaturation, all collapsed in practically the same curve when plotted in terms of the single parameter Ca.

Typical patterns at different growth stages are shown

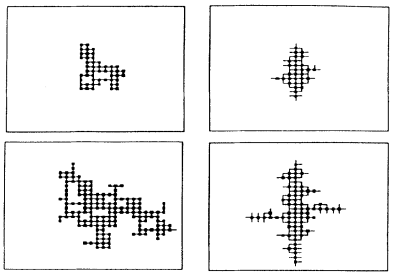

(a) Capillary Control (b) Viscous Control

FIG. 7. Typical sequence of gas cluster growth under conditions of (a) capillary control (Ca=0.000 01) and (b) viscous control (Ca=0.1).

in Fig. 7, under conditions of percolation [Fig. 7(a)] or viscous [Fig. 7(b)] control. [The anisotropy of the pattern of Fig. 7(b) reflects the anisotropy of the underlying square lattice.] The patterns are fully consistent with the theory. One should notice that in the viscous fingering regime, multiple pores are allowed to be penetrated simultaneously, which is in contrast to the percolation regime, where only one bond is penetrated at each time. Finally, the scaling of the rate of growth [Eq. (36)] was tested (Fig. 8). The numerical results appear to agree quite well with the predicted linear scaling. More stringent tests of these predictions would require simulations in larger and 3D lattices to minimize finite-size effects.

The previous scalings rely on the assumption of quasistatic mass transfer, which is equivalent to the condition

$$\mathrm{Ja}\left|\frac{\partial C}{\partial t}\right| \ll \left|\frac{\partial^2 C}{\partial r^2}\right| . \tag{39}$$

Using the mean-field results, this condition can be quantitatively expressed. For example, the concentration profile in 3D is

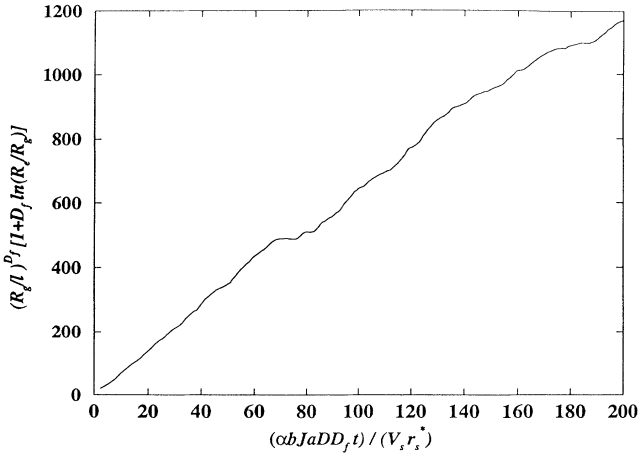

FIG. 8. Scaling of bubble growth in 2D geometries from pore network simulations. A linear time scaling is predicted from Eq. (36).

$$C = C_0 - (C_0 - C_i)\frac{R_g}{r} . \tag{40}$$

For growth in the bulk, it can be readily shown that condition (39) translates into $\mathrm{Ja} \ll 1$. For growth in a porous medium, however, the constraint is not as apparent. Substitution of (40) into (39) and evaluation at $r = R_g$, in combination with (38), shows that for the quasistatic limit to apply in this case requires [5] $\mathrm{Ja}t^{(3-D_f)/(D_f-1)} \ll 1$. In other words, in fractal patterns ($D_f < 3$) the quasistatic condition becomes *time dependent.* Since the limiting sizes R^p and R^{vf} are known, however, we can still test whether the bulk condition $\mathrm{Ja} \ll 1$ remains applicable when these limits are reached, as was tacitly assumed above. To proceed, we combine (28) or (33) with (37) and insert the result in (39) to give $\mathrm{Ja}^{1-[\nu/(\nu+1)](3-D_f)} \ll 1$ or $\mathrm{Ja}^{1-[D_f(3-D_f)/(D_f-1)]} \ll 1$, for the percolation or viscous fingering boundaries, respectively. Since $D_f \sim 2.5$ in either pattern, we conclude that the condition $\mathrm{Ja} \ll 1$ remains uniformly valid in this case.

The above theory is also useful in determining limiting patterns and rates of growth for the problem involving a constant rate of decline of the far-field pressure $a = -dP_\infty/dt$. This is commonly encountered in applications of oil recovery by "solution gas drive" [1]. Although the effective supersaturation is time dependent, the problem can still be described with the previous quasistatic theory by using a *time-dependent Jakob* number, $\mathrm{Ja} = at$. Now, assuming that the quasistatic regime holds, all previous expressions apply, provided that the appropriate modification for Ja (and Ca) is inserted in the various equations. A direct consequence is that both percolation and viscous fingering boundaries now become time dependent. To test the validity of the quasistatic approximation we follow the previous approach. For example, after some algebra one can find the following condition for the validity of the quasistatic regime when the percolation boundary is reached [5]:

$$\left[\frac{a r_p^{*2}}{D P_0}\right]\left[\frac{D\mu l}{\gamma k}\right]^{-\{\nu(D_f-1)/[\nu(1+D_f)+2]\}} \ll 1 . \tag{41}$$

For typical parameter values in oil reservoir applications ($a \sim 1$ psi/day, $P_0 \sim 1000$ psi, $D \sim 10^{-5}$ cm^2/s, $\mu_l \sim 1$ cp, $r_p^* \sim 1$ μm, and $\gamma \sim 60$ dyn/cm) this condition is readily satisfied. On the other hand, larger pressure decline rates and lower far-field pressures (e.g., application of vacuum) lead to an early violation of this regime.

IV. CONCLUSIONS

In this paper a scaling theory was developed for the patterns and rates growth of a single gas cluster in a porous medium as a result of an applied far-field supersaturation. The process considered corresponds to low supersaturations, where diffusion predominates. It was shown that the following regimes develop in succession: a short duration early-time regime, where finite-size effects predominate, the growth is still compact, and the classical effective medium scaling is applicable; an invasion percolation regime $R_g \leq R^p$, where the cluster

originates from the nucleation site and the growth is "one site at a time;" a transition to a viscous fingering regime, $R^p \leq R_g \leq R^{vf}$; and a DLA regime, $R^{vf} \leq R_g$, where growth occurs at multiple sites at the same time and is controlled by viscous forces. Scalings for the pattern boundaries and growth rates were determined in the absence of convection (low Ja) in terms of the imposed supersaturation, expressed through a diffusion-based capillary number, Ca. The scaling of the rate of growth was found to be different than the classical scaling and to obey in 3D the law $R_g \sim t^{1/(D_f-1)}$, with logarithmic corrections for the case of a 2D geometry. The above results are based on the absence of gravity or of capillary instabilities, such as snap-off of gas bubbles in pore throats. These, as well as effects of convection (larger Ja) or of an externally imposed velocity field, are currently under study (see also [8]).

ACKNOWLEDGMENTS

This work was supported in part by DOE Contract No. DE-FG22-90BC14600 and by a grant from Chevron Petroleum Technology Corporation. These sources of support are gratefully acknowledged.

APPENDIX

In 2D geometries, the liquid phase cannot simply be connected, since the simultaneous percolation of two phases is not possible in two dimensions. To calculate the pressure drop between the growing site at point A (Fig. 2) and another site at point B at the opposite side of the cluster, the percolation vapor cluster must be considered "opaque" rather than "transparent," as is the case in 3D, to be discussed below. To proceed with an effective medium solution, we approximate the cluster as a compact circle of radius R_g, the boundary of which is impermeable to fluid flow, and consider the pressure field induced by a point source of a given strength q at point A of the perimeter (Fig. 9). The solution of this problem can be obtained as a special case of the more general problem considered by Lamb [15], where the source is at an external point P (Fig. 9). To solve the latter, an imaginary source and an imaginary sink of strength q are placed at points Q and O, respectively, where Q is the inverse point of P (satisfying $R_g^2 = |OP||OQ|$) and O is the center of the circle, in which case one can readily show that the perimeter becomes a no-flow boundary. Then, by taking the limit $P \to A^+$, $Q \to A^-$, the solution for the complex potential W is

$$W \equiv \phi + i\psi = -q \ln(z - z_{A^-}) - q \ln(z - z_{A^+}) + q \ln z = -q \ln \frac{(z - z_{A^-})(z - z_{A^+})}{z} , \quad \text{(A1)}$$

where ϕ is the potential, ψ is the stream function,

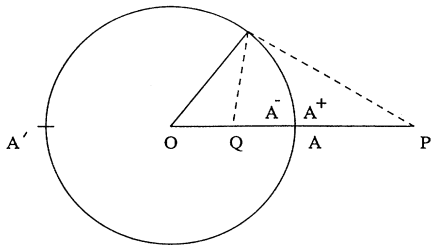

FIG. 9. Geometric construction for the solution of a potential flow problem around a circle with point source A. The solution is obtained as the limit when $P \to A^+$, $Q \to A^-$, where Q is the inverse point of P.

$z = re^{i\theta}$, and $z_A^{\pm}$ ($z_{A^-} = R_g - l$, $z_{A^+} = R_g + l$) denotes the position of $A^{\pm}$. The real part of (A1) yields the potential

$$\phi = -q \ln R , \quad \text{(A2)}$$

where

$$R^2 = \left[\cos\theta \left(r + \frac{R_A^2 - l^2}{r} \right) - 2R_g \right]^2 + \sin^2\theta \left(r - \frac{R_g^2 - l^2}{r} \right)^2 . \quad \text{(A3)}$$

Typical isopotential curves shown in Fig. 4(b) show a qualitative similarity to the constant pressure curves obtained from simulation of the actual problem [Fig. 4(a)]. The maximum potential drop on the circle perimeter occurs at the point A', antidiametric to A. The potential drop can be readily evaluated using (A2) and (A3) by considering points with $\theta = 0$, $r = R_g$ and $\theta = \pi$, $r = R_g$. Then,

$$\Delta\phi = q \ln \left(1 + \frac{4R_g^2}{r_s^{*2}} \right) , \quad \text{(A4)}$$

where we approximated $l \approx r_s^*$. By transforming to the dimensional variables used in the text, we get

$$\Delta P_v \approx \frac{v_m \mu r_s^*}{k} \ln \left(1 + \frac{4R_g^2}{r_s^{*2}} \right) , \quad \text{(A5)}$$

which in the large R_g / r_s^* limit gives

$$\Delta P_v \approx \frac{2v_m \mu r_s^*}{k} \ln \left(\frac{2R_g}{r_s^*} \right) . \quad \text{(A6)}$$

This is Eq. (15) in the main text.

For 3D geometries, the liquid phase is connected so that the gas cluster is "transparent" to the fluid flow calculation. We may then approximate this problem as spherically symmetric flow from a point source, which yields (16) in the text, in a straightforward manner.

[1] E. B. Hunt, Jr. and V. M. R. Berry, AIChE J. **2**, 560 (1956); J. M. Dumore, SPE J. **10**, 211 (1970); C. H. Sondergeld and L. Turcotte, J. Geophys. Res. **82**, 2045 (1977); J. R. Thome, *Enhanced Boiling Heat Transfer* (Hemisphere, New York, 1990).

[2] E. Yousfi, C. Zarcone, S. Bories, and R. Lenormand, C. R. Acad. Sci. Ser. II **313**, 1093 (1991).

[3] L. E. Scriven, Chem. Eng. Sci. **10**, 1 (1959); M. S. Plesset and A. Prosperetti, Ann. Rev. Fluid Mech. **9**, 145 (1977); X. Li and Y. C. Yortsos, Phys. Fluids A **6**, 1663 (1994).

[4] D. Wilkinson and J. F. Willemsen, J. Phys. A **16**, 3365 (1983); R. Lenormand, J. Phys. Condens. Matter **2**, SA79 (1990).

[5] X. Li and Y. C. Yortsos, Chem. Eng. Sci. (to be published); AIChE J. (to be published).

[6] J. Szekely and G. P. Martins, Chem. Eng. Sci. **26**, 147 (1971); J. Szekely and S. D. Fang, *ibid.* **28**, 2127 (1973).

[7] Y. C. Yortsos and M. Parlar, *SPE 19697, Proceedings of the 64th Annual Conference on the Society of Petroleum Engineers* (Society of Petroleum Engineers, Richardson, Texas, 1989).

[8] C. Satik and Y. C. Yortsos, J. Heat Transfer (to be published).

[9] I. M. Lifshitz and V. V. Slyozv, J. Phys. Chem. Solids **19**, 35 (1961).

[10] A. J. Katz and A. H. Thompson, Phys. Rev. B **34**, 8175 (1987).

[11] B. Sapoval, M. Rosso, and J. F. Gouyet, J. Phys. (Paris) Lett. **46**, L419 (1985); J. F. Gouyet, M. Rosso, and B. Sapoval, Phys. Rev. B **37**, 1832 (1988); M. Chaouche, N. Rakotomalala, D. Salin, B. Xu, and Y. C. Yortsos, Phys. Rev. E **49**, 4133 (1994).

[12] M. E. Cates and T. A. Witten, Phys. Rev. A **35**, 1809 (1987).

[13] R. Lenormand, Proc. R. Soc. London Ser. A **423**, 159 (1989).

[14] J. S. Langer, Rev. Mod. Phys. **52**, 1 (1980); *The Dynamics of Curved Fronts,* edited by P. Pelce (Academic, New York, 1988).

[15] H. Lamb, *Hydrodynamics* (Dover, New York, 1945).

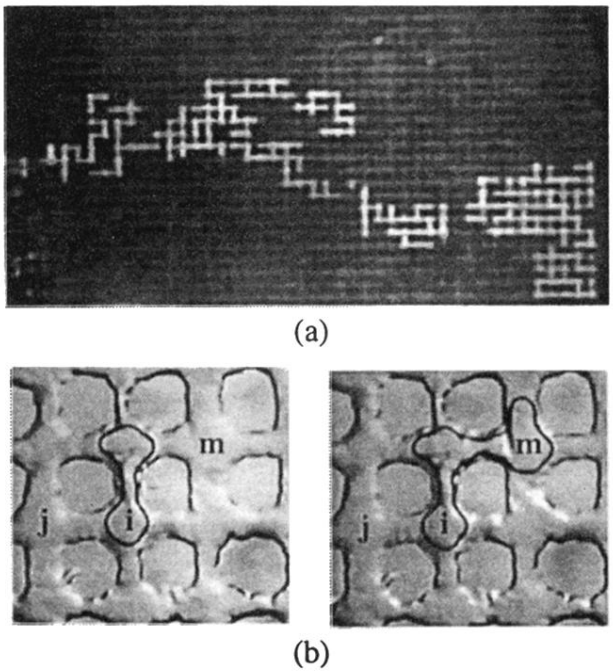

FIG. 1. Experimental snapshots of gas cluster growth from carbonated water in a glass micromodel: (a) large scale; (b) pore scale sequence.

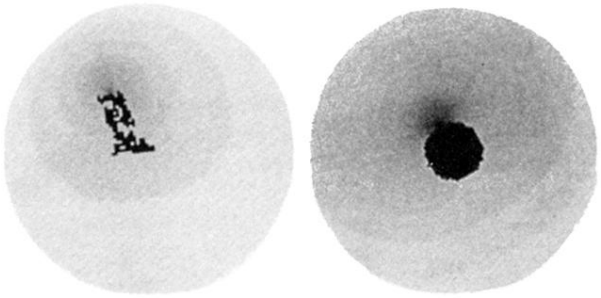

(a) (b)

FIG. 4. Pressure fields corresponding to bubble growth: (a) full numerical simulation; (b) mean-field result.